5 Calcium Zirconium Silicate (Baghdadite) Zinc Oxide composite system

5.1 Introduction

Calcium silicate (Ca–Si) based ceramics have good bioactivity, mechanical properties, and bone growth ability that makes it a suitable candidate for bone graft substitutes (Sadeghpour et al., 2014). The substitution of Zr ion developed a stable Calcium silicate-based material known as calcium zirconium silicate or baghdadite ($Ca_3ZrSi_2O_9$). It shows non-toxicity on osteoblast cells and makes them applicable for tissue engineering (Ramaswamy et al., 2008). But it's inferior antibacterial activity results infection in implant and produces postoperative complications (Bakhsheshi-Rad et al., 2017). Studies suggest that the bone formation rate in baghdadite is faster than calcium magnesium silicate (Najafinezhad et al., 2017), β-TCP microbeads, and Hap/β-TCP scaffold (Luo et al., 2012). For biomedical applications, both mechanical, as well as biological properties are significant parameters. The changes in the composition of bone substitute biomaterials lead to an improvement in both variables. The incorporation of trace elements into the structure leads to the changes in chemical nature of the material. Schumacher et al., 2015 developed Sr-doped baghdadite scaffold by a freeze-casting method and evaluated the effect of doping on osteoblast proliferation and ALP activity. Results showed that doping does not affect the mechanical property while the ALP activity of HOBs increases with Sr-amount. H. R. Bakhsheshi-Rad et al., 2017 studied the effect of coating on zinc oxide/calcium zirconium silicate over Mg alloy. The corrosion resistance, bioactivity, and antibacterial properties of the zinc oxide/calcium zirconium silicate-coated substrate found better than zinc oxide coated substrate. Various literatures reported the effect of Zn on the structure and properties of bioceramics. It stimulates osteoblast proliferation and differentiation to improve the bone-bonding ability of implant (Kazemi et al., 2017, Luo et al., 2012). It has antibacterial properties against both gram-negative and gram-positive bacteria. It also used as a food preservative agent, packaging, water purification, and drug delivery (Ali et al., 2020). The

baghdadite ceramic suffers from poor antibacterial activities. The most common problem in an orthopedic implant is an infection caused by bacterial adhesion and colonization on the implant or adjacent tissues. For this, zinc oxide was incorporated in baghdadite to inhibit bacterial adhesion. There is limited research available on the incorporation of metal oxides in baghdadite. In present work, the calcium zirconium silicate/ZnO composites prepared by a solid-state method followed by sintering to analyze the effect of substitution on antibacterial and biological properties.

5.2 Materials and method

5.2.1 Synthesis of baghdadite/zinc oxide composite

For baghdadite or calcium zirconium silicate synthesis, a solid-state ceramic synthesis route was selected. Calcium carbonate, zirconium oxide, and quartz were selected. All reagents were weighed in an appropriate weight to maintain the molar ratio of calcium oxide: zirconium oxide: silica is 3:1:2. For composite synthesis, zinc oxide powder used to partially substitute calcium. Weighted reagents were mixed and ball-milled. Milled powder sintered. Table 5.1 shows the sample code with the zinc oxide in baghdadite.

Table 5.1 Sample code with zinc oxide amount.

Sample Code	ZnO (mol %)
CaZn0	0
CaZn0.1	0.1
CaZn0.25	0.25
CaZn0.5	0.5

5.3 Thermal analysis

For thermal analysis, differential scanning calorimetry (DSC) and thermogravimetry (TGA) were used. The composite powder was heated up to 1000°C with a heating rate of 10°C/min under the nitrogen atmosphere.

5.4 Phase, structural, and microstructure analysis

Phase analysis and structure of composite powder was carried out by the X-ray diffractometer with the filtered CuKα radiation (λ = 0.154 nm) in the 2θ range of 20-70° was utilized (step size = 0.02°). The obtained diffraction pattern was analyzed with the JCPDS file to identify the phases. FT-IR was utilized to determine the functional group present in the composite samples before and after immersion in SBF in the range of 400-2000 cm^{-1} using ATR Fourier transform infrared spectroscopy. SEM with elemental mapping was analyzed to determine morphology, apatite formation ability, and elemental composition on scanning electron microscopy at an acceleration voltage of 30 kV. Pallet of 10 mm× 2 mm dimension was gold coated on carbon tape for SEM analysis.

5.5 In-vitro bioactivity and chemical analysis

The In-vitro bioactivity of composites was analyzed by forming an apatite layer on the surfaces during immersion in SBF. The chemical analysis of samples examines the degradation rate, pH change, and water absorption during immersion in SBF. SBF is a solution which has ion concentration similar to blood plasma. For this, a cylindrical sample of size 10 mm dia and 2 mm thickness immersed in SBF for 7, 14, 21, and 28 days. The ratio of SBF solution to pallet weight kept 100:1 (Yadav et al., 2020). During this interval, the pH value noticed. A pH-meter used to measure the pH values. The bioactive behavior was measured by analyzing the resulted apatite layer formation using XRD, FTIR, and SEM-EDX

techniques. The in-vitro degradation rate was measured in terms of weight loss with immersing time in SBF by equation (3.1 and 3.2).

For each composite, weight measured three times, and their mean weight loss calculated.

5.6 Density and compressive strength

For density measurements, the powder uniaxially pressed in a hydraulic press at 10-ton pressure for 90s to obtain a green body of dimension 10×2 mm^2. The green body sintered in a two-step heat treatment process with heating and cooling rate of 2°/min. Firstly, the green body was heated up to 500°C to remove any possible residue and then heated at different temperature 800, 900, 1000, 1100, and 1200°C to achieve maximum relative density. The density of composites has evaluated by the Archimedes principle. For this, sintered pallets were prior dried at 70°C. The bulk density of composites was calculated according to equation (3.4).

A Compressive test performed on cylindrical samples of dimension 10×9 mm^2 sintered at 800°C using Tinius Olsen H10KL UTM with a crosshead speed of 0.5 mm/min**.** Triplicates of each composition were selected and averaged their value. The compressive strength of composites sample was calculated according to equation (3.3).

5.7 In-vitro blood compatibility

The hemolytic activity of composite was measured according to the method described as ASTM F 756-00 (ASTM, 2000). For error minimization, triplicates of each sample were taken to average their optical density values. The hemolysis rate (%) was calculated by equation (3.9) (Hossain et al., 2020).

The obtained results are compared with the ASTM standard. The composites are assigned as non-hemolytic for <5% hemolysis rate and hemolytic for >20 % hemolysis rate (Ali et al., 2018).

5.8 Apoptosis analysis

To examine MG-63 cell proliferation on the baghdadite composites, nuclear staining with DAPI (4′,6-diamidino-2-phenylindole) was performed under fluorescence microscopy. The MG-63 cells were seeded on culture plates as a control for 24hr.

5.9 In-vitro antibacterial test

The antibacterial behavior of composites was observed over *E. Coli* (MTCC#1673) and *S. aureus* (MTCC#435) bacterial strain using MTT (3(4,5- dimethylthiazol-2-Yl)-2,5-diphenyl tetrazolium bromide) assay. To perform the antibacterial test, three pallets of size 10×2 mm^2 for each composition were selected. The viability and antibacterial effect over both bacterial strains were calculated from equation (3.10).

5.10 Statistical analysis

For in-vitro antibacterial test and blood compatibility analysis, triplicates of each sample were performed and data were presented as mean with standard deviation (mean ± SD). The one-way ANOVA test followed by Tukey's post hoc test was used for significance differences (p-value < 0.05).

5.11 Results and discussion

5.11.1 Thermal analysis

Figure 5.1 shows the thermal analysis of composite powder. From TG analysis, in the CaZn0 sample, the weight of raw powders exhibit a continuous decrease from 564°C to 747°C, and the total weight loss was about 22.87 %. Also, in sample CaZn0.1, CaZn0.25, and CaZn0.5, the total weight loss was 23.55, 22.45, and 20.59 %. The theoretical weight loss was also calculated and found about 24.28 %, 24.38 %, 23.18%, and 21.13 % for

sample CaZn0, CaZn0.1, CaZn0.25, and CaZn0.5. The TG graph becomes stable after 750°C which indicates no weight loss and complete formation of calcium zirconium silicate (Yadav et al., 2019).

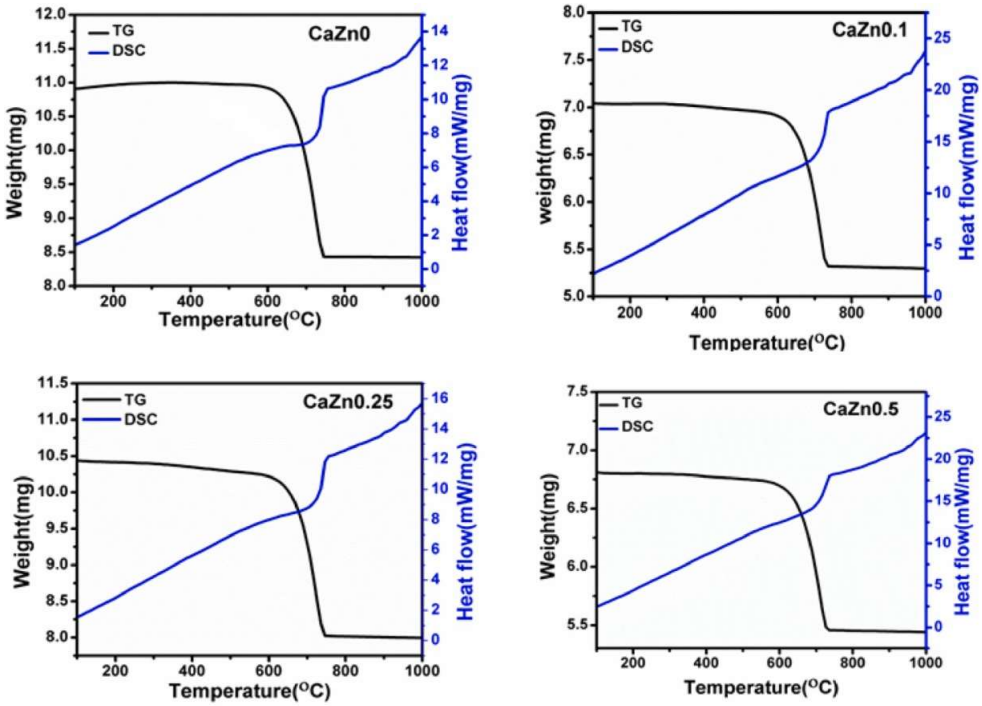

Figure 5.1 Thermal analysis of doped and undoped raw powder.

5.12 Phase, structural, and microstructural analysis

XRD was used to evaluate the phase composition and structure of composite samples. **Figure 5.2** shows the diffraction pattern of baghdadite/zinc oxide composite prepared at 1300°C confirmed the baghdadite (reference code 98-003-3844) of a monoclinic structure. Zinc oxide substituted powders were sintered at 1400, 1350, and 1300°C but no phase formation of baghdadite was found at 1350 and 1400°C (not shown in fig). In zinc oxide substituted samples, the diffraction pattern indicates the calcium zirconium silicate formed with a zinc oxide wurtzite type of hexagonal structure (reference code 98-011-4665).

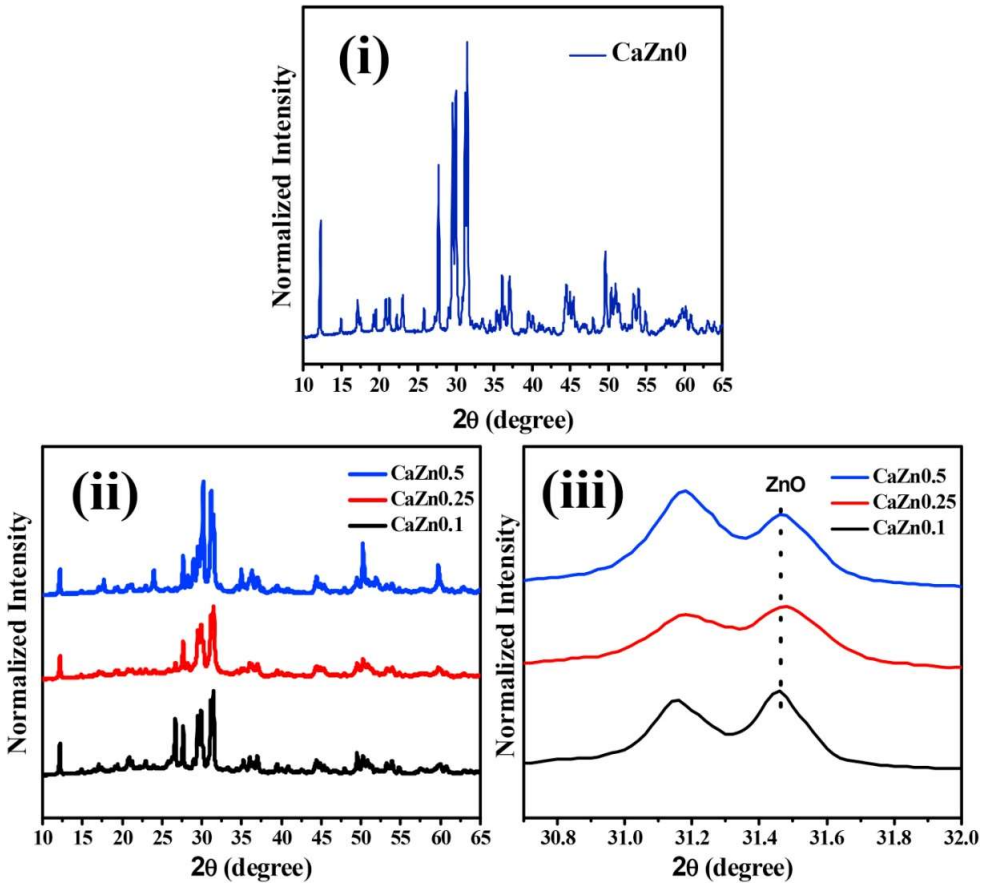

Figure 5.2 XRD pattern of **(i)** baghdadite **(ii)** zinc oxide doped baghdadite **(iii)** ZnO peaks in at 2θ of 31.4° in doped baghdadite samples.

Figure 5.3 shows the functional group present in baghdadite composites. Transmittance bands in the range of 973, 948, 918, 860, 634 cm^{-1} are related to the Si-O band. The Si-O-Zr band appeared at 1036 cm^{-1}. Further, the Ca-O absorption band was formed at 511 and 460 cm^{-1} (Sadeghpour et al., 2014, Najafinezhad et al., 2017, Sadeghzade et al., 2020). The Zn-O stretching bond was formed at 454 cm^{-1} in zinc-containing baghdadite (Bakhsheshi-Rad et al., 2017).

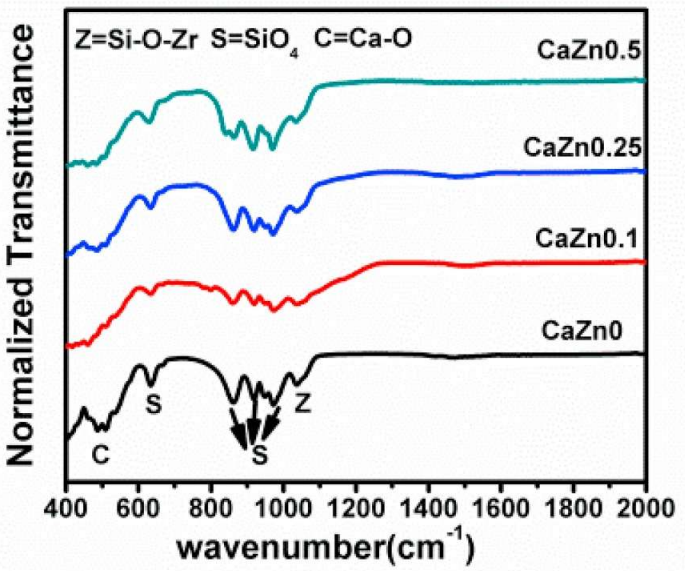

Figure 5.3 Transmittance FTIR of baghdadite composite.

Figure 5.4, **Figure 5.5**, **Figure 5.6**, and **Figure 5.7** shows the microstructure of composite with the elemental mapping of Ca, Zr, Si, and Zn. In SEM images, all samples show agglomerated and dense structure. Clear changes in microstructure have found in samples, mainly due to differences in the composition of each sample. In elemental mapping, the composing elements of composites were presented and homogeneously distributed in samples.

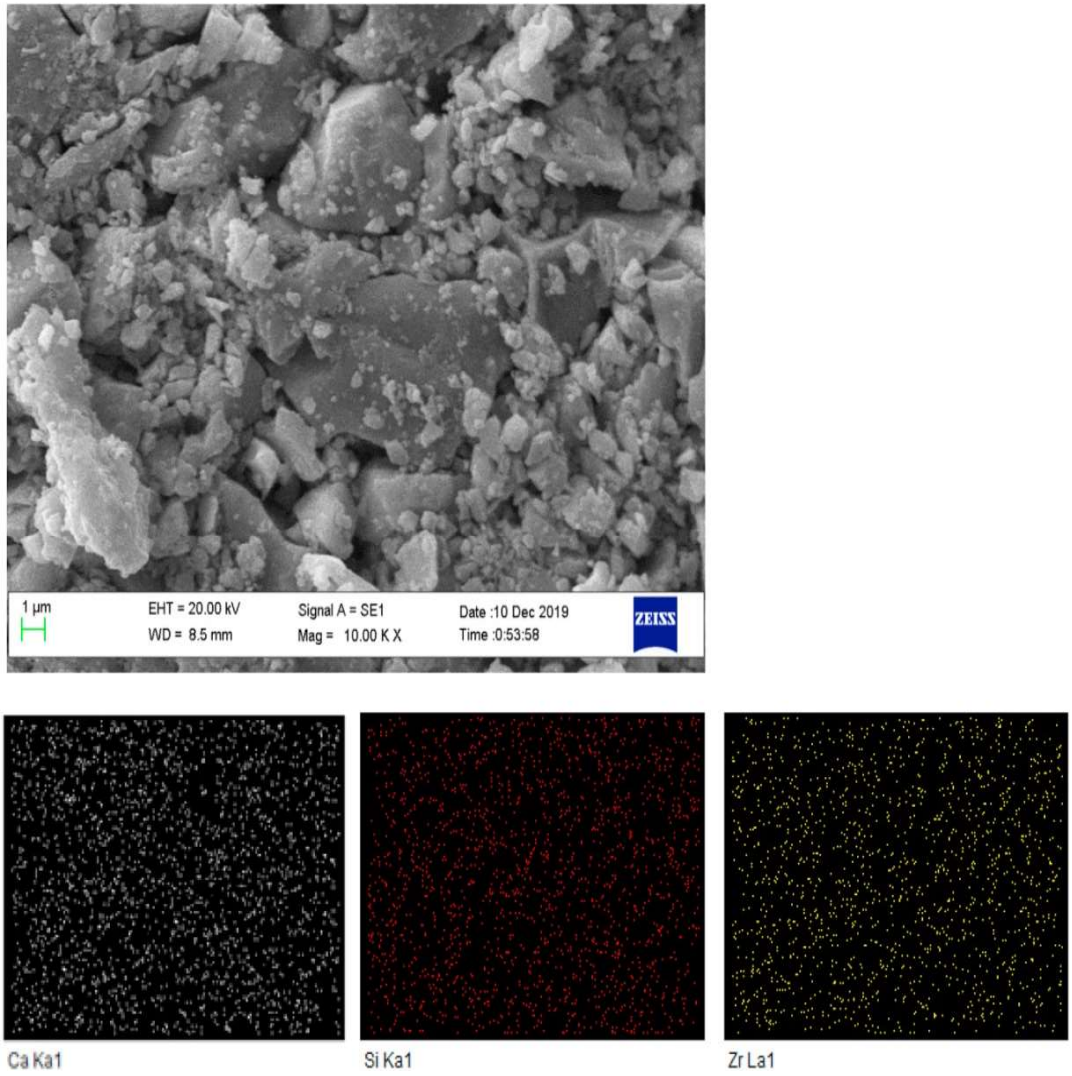

Figure 5.4 SEM with elemental mapping of prepared CaZn0 sample sintered at 800°C.

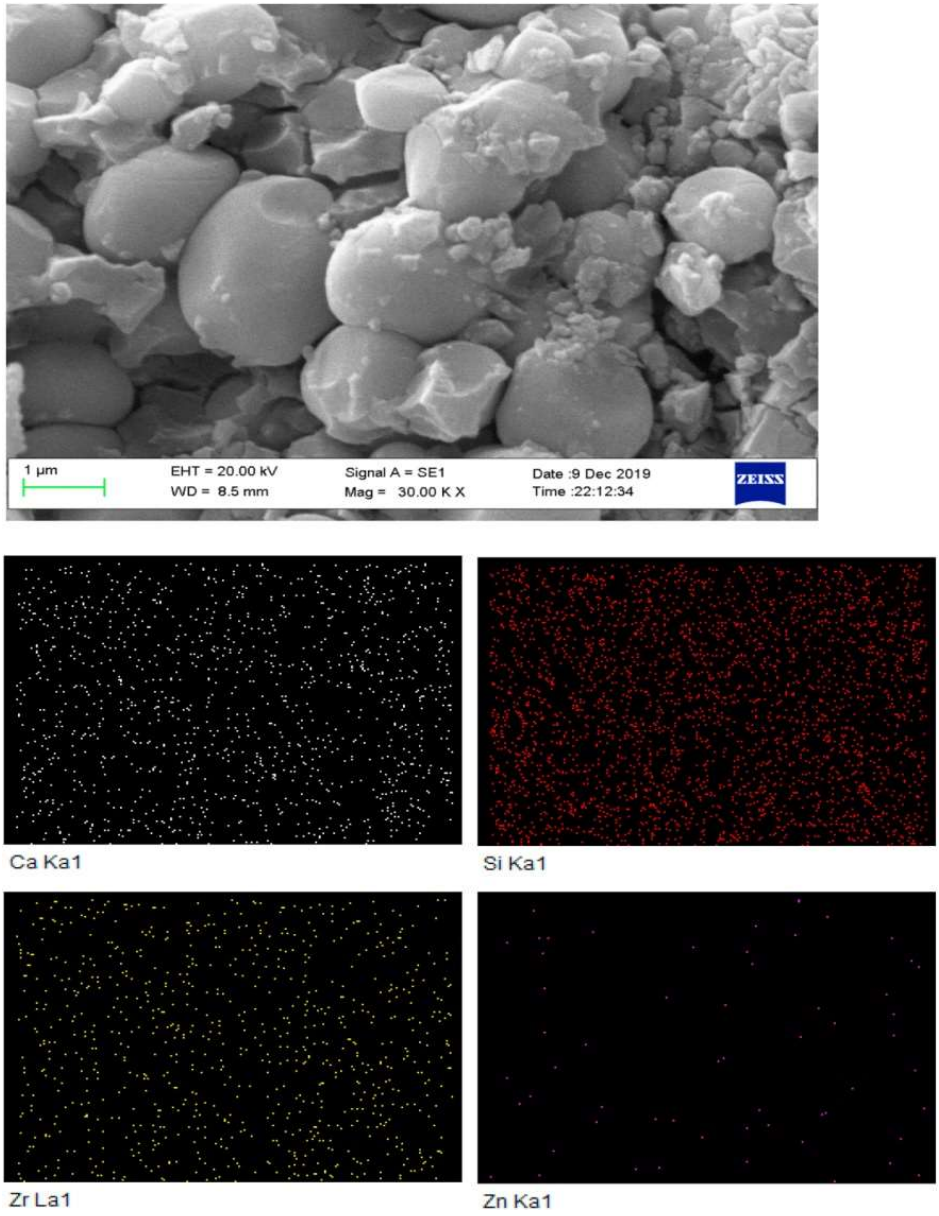

Figure 5.5 SEM with elemental mapping of prepared CaZn0.1 sample sintered at 800 °C.

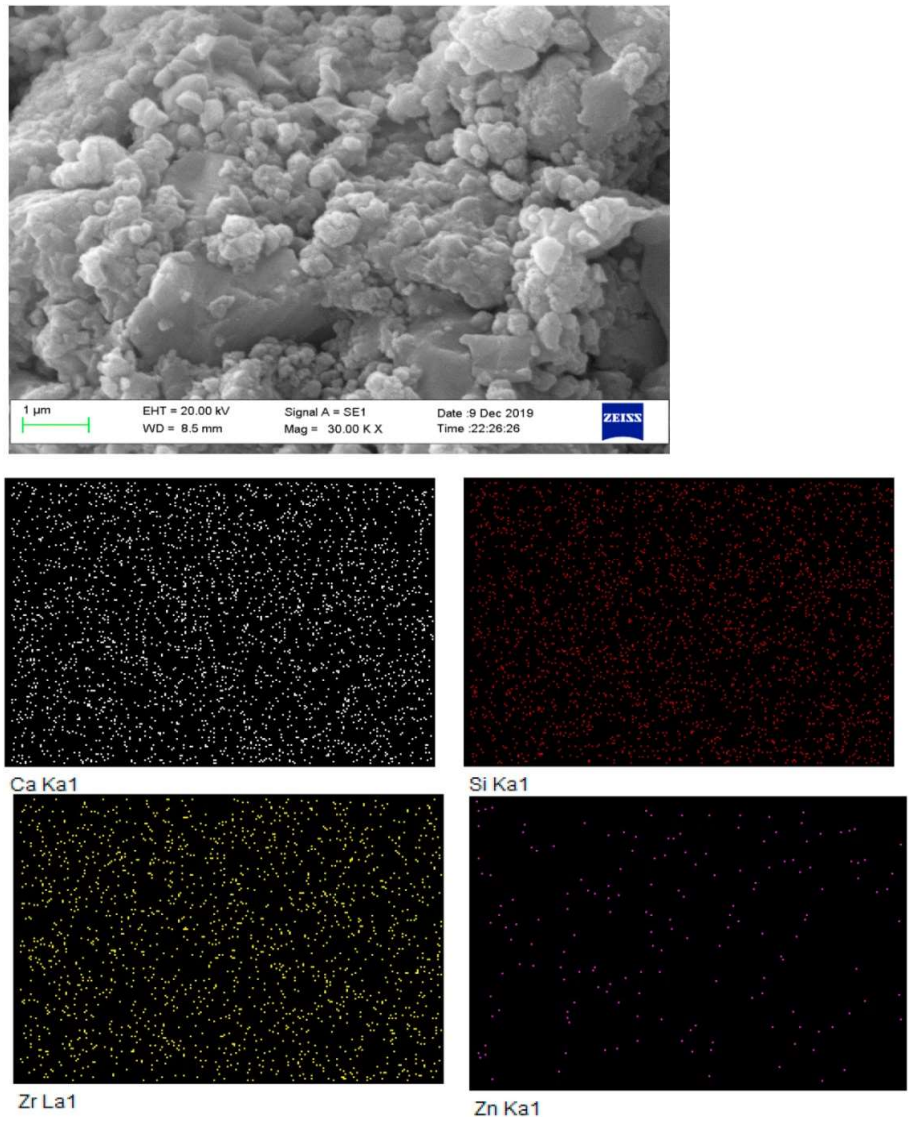

Figure 5.6 SEM with elemental mapping of CaZn0.25 sample sintered at 800°C.

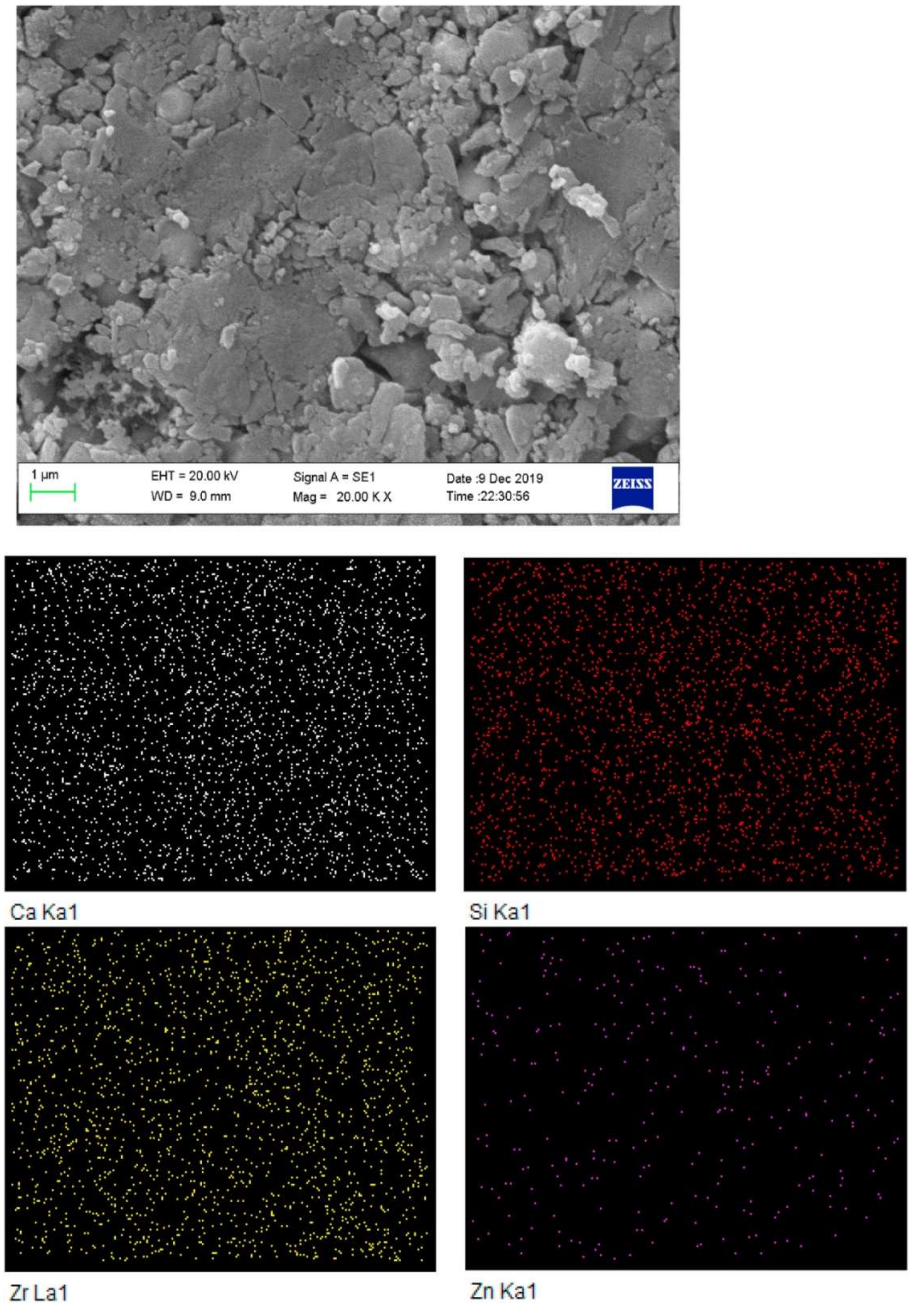

Figure 5.7 SEM with elemental mapping of prepared CaZn0.5 sample sintered at 800°C.

5.13In-vitro bioactivity analysis

In-vitro bioactivity was measured to analyze the in-vivo bone formation ability of biomaterials. The hydroxyapatite layer formation over the sample surface during immersion in the SBF was analysed for 28 days. The formation of hydroxyapatite in bioactive materials helps to connect with neighboring tissues. In other words, hydroxyapatite formation is necessary for the combination of bone tissue to bioactive materials. Apatite formation over baghdadite and composite surface during immersion in the SBF were evaluated by FTIR, XRD, and SEM coupled with EDS. To measure in-vitro bioactivity, SBF, and culture media method is used in which the SBF method is generally used (Sadeghzade et al., 2017).

Figure 5.8 presents the XRD pattern of composites after immersion in SBF for 7, 14, 21 and 28 days. The peak of crystalline hydroxyapatite at $2\theta = 31.7°$ is observed in the XRD pattern after immersion in SBF. All samples show a crystalline hydroxyapatite phase after 7 days of immersion in SBF. The sharp peaks at $2\theta = 26°$ and $29°$ confirms the transition of amorphous calcium phosphate into crystalline hydroxyapatite (Schumacher et al., 2015).

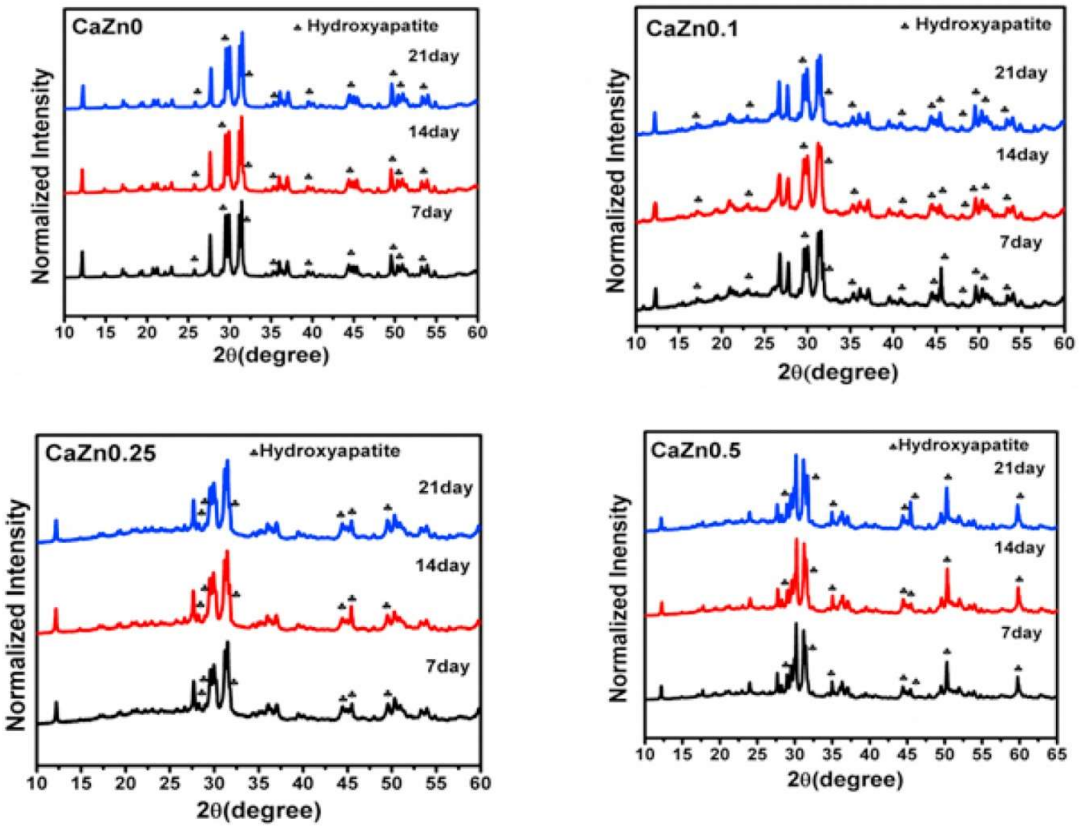

Figure 5.8 XRD pattern of composites after immersion in SBF for different time interval.

Figure 5.9 shows the FTIR analysis of composite for 7, 14, 21, and 28 days immersion in SBF. The phosphate bands of vibration mode formed at 491, 515, and of stretching mode at 919-1035 cm^{-1} confirm the formation of hydroxyapatite after immersion. During immersion, the intensity of Si-O-Zr and Ca-O were tended to reduce and replaced by a newly formed phosphate group which indicates the hydrolysis of metal ions during immersion (Bakhsheshi-Rad et al., 2017, Yadav et al., 2020). The twin band of a phosphate group at 491 and 515 cm^{-1} shows the crystalline nature of hydroxyapatite (Schumacher et al., 2015). The apatite formation in baghdadite ceramics depends upon the ion exchange into SBF. Calcium zirconium silicate is SiO_4^{-4} type and makes a fast hydrolysis reaction in SBF. During SBF immersion, Ca^{+2} ions rapidly transfers into the solution increasing the Ca^{+2} ion concentration. Also, Si^{+2} ions from calcium zirconium silicate show the same behavior at a

slow rate. Consumption of Ca^{+2} and P ions form apatite on the sample surface. The formation of the amorphous apatite layer is because of the decrease in P ions concentration during the ion transfer process. In other words, apatite formation on the surface of the bioceramic occurs due to the nucleation and growth process (Sadeghpour et al., 2014, Schumacher et al., 2015, Xiong et al., 2013).

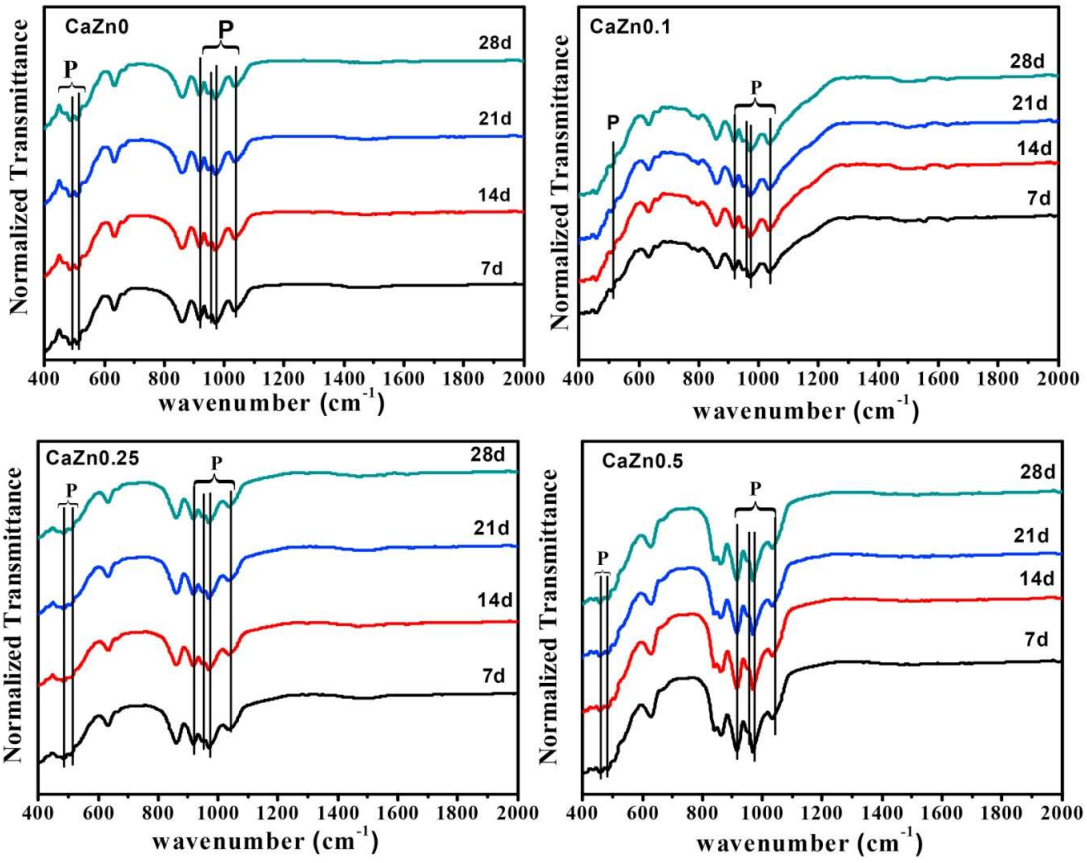

Figure 5.9 FTIR of composites after immersion in SBF for different time interval (P indicate the phosphorus peak)

Figure 5.10, **Figure 5.11**, **Figure 5.12**, and **Figure 5.13** shows the SEM images with the elemental mapping of samples after immersion in SBF for 28 days. In SEM images, the deposition of a new phase over the sample surface was seen and confirmed in elemental mapping also. The morphology of precipitates formed over the surface was different and vary with the zinc oxide amount. In calcium zirconium silicate (CaZn0) sample, needle-like

surface covered the sample. In elemental mapping, the presence of Ca and P exists over the surface. Since calcium zirconium silicate is P free; the existence of P in elemental mapping confirms the formation of calcium phosphate after immersion. The release of ions from the sample is also necessary for the hydroxyapatite formation. In elemental mapping, all elements (Ca, Zr, Si, Zn, and P) are distributed homogeneously over the surface.

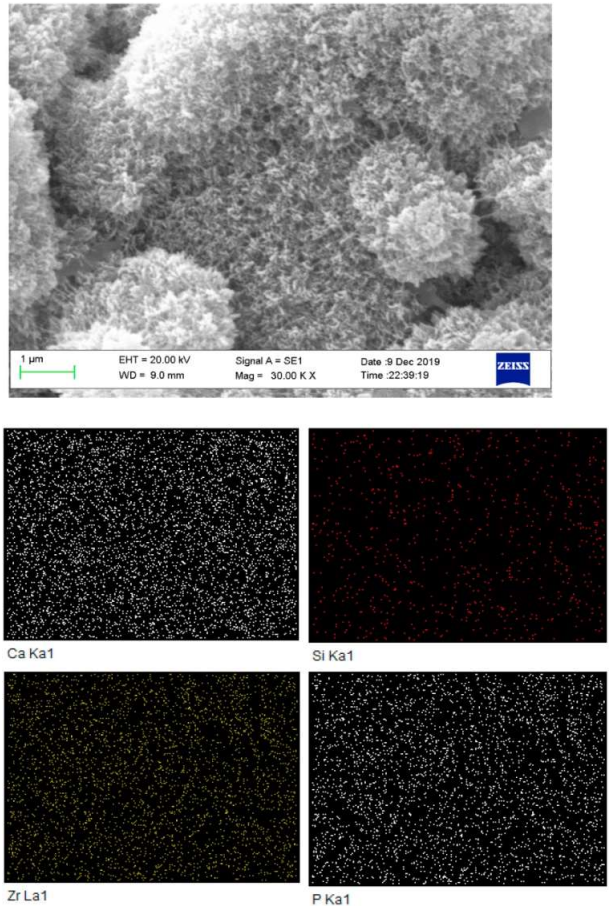

Figure 5.10 SEM with elemental mapping of CaZn0 sample after 28 days of immersion in SBF.

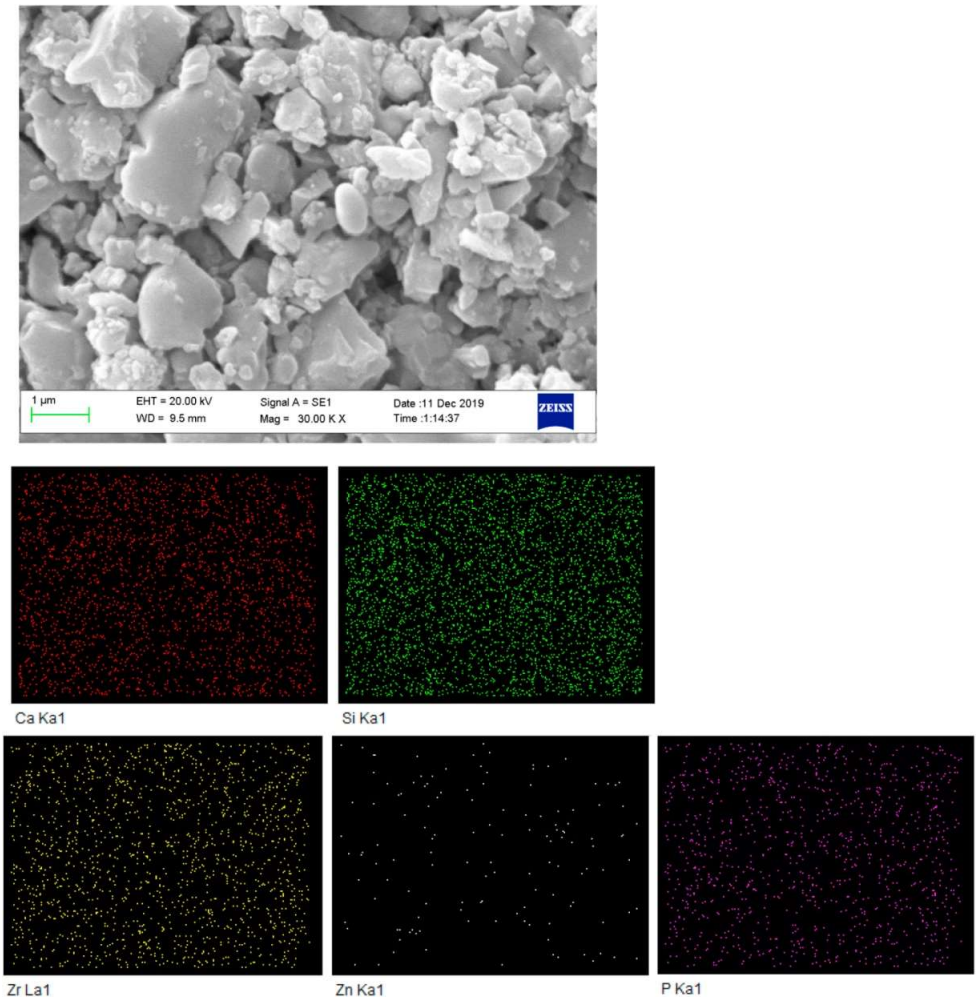

Figure 5.11 SEM with elemental mapping of CaZn0.1 sample after 28 days of immersion in SBF.

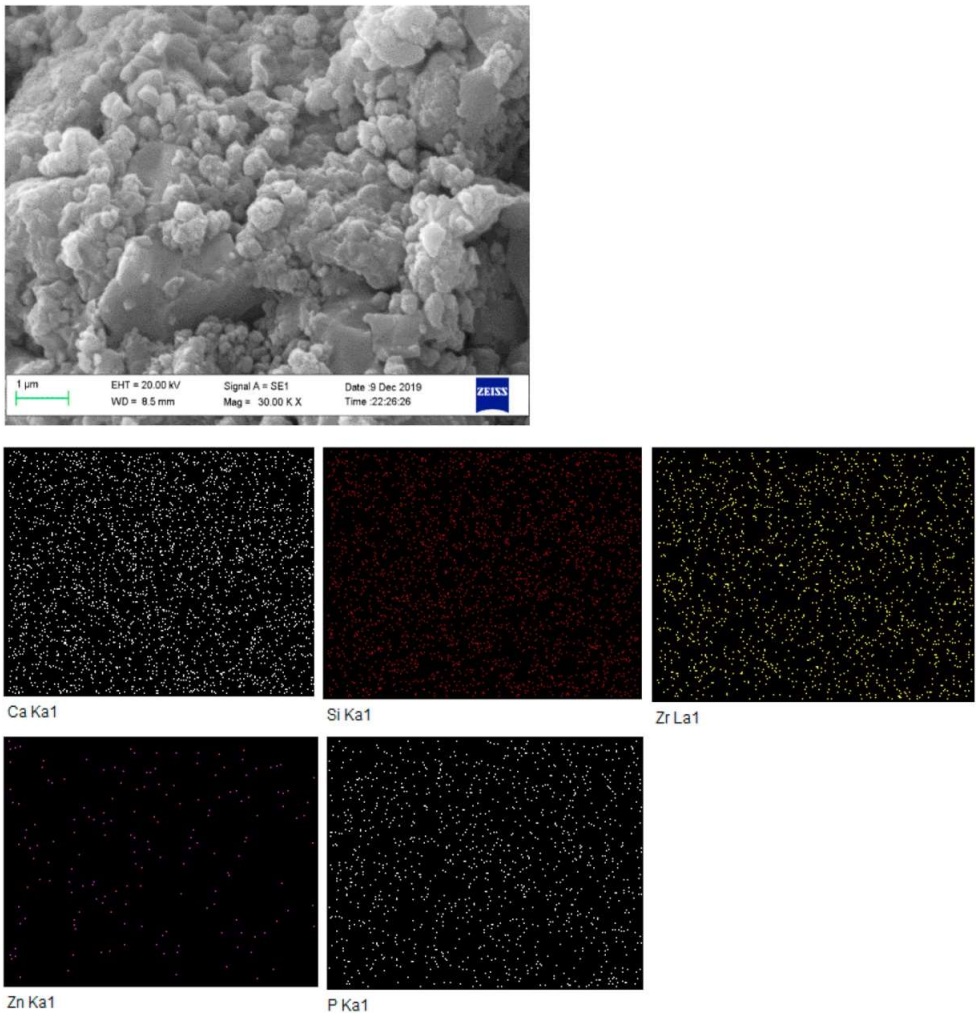

Figure 5.12 SEM with elemental mapping of CaZn0.25 sample after 28 days of immersion in SBF.

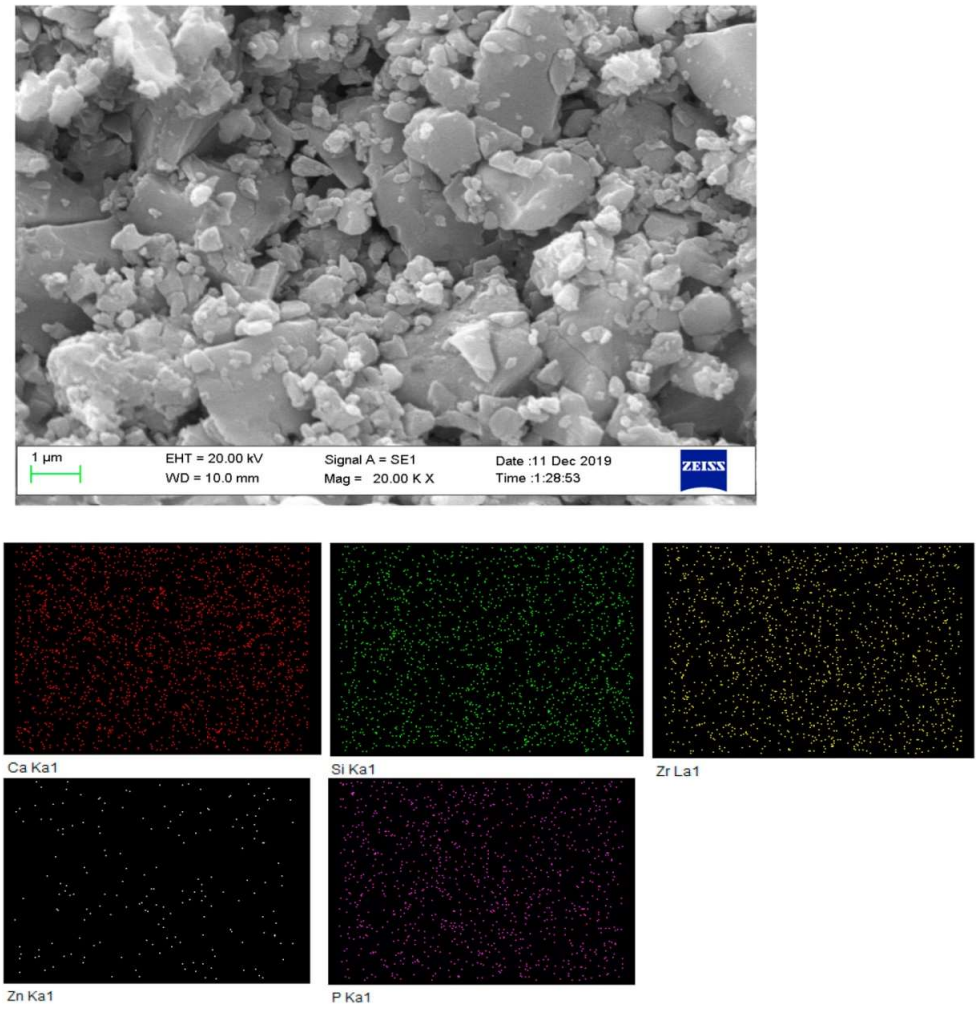

Figure 5.13 SEM with elemental mapping of CaZn0.5 sample after 28 days of immersion in SBF.

5.14 Chemical analysis

Figure 5.14 present the variation in the pH of composite samples after immersion in SBF. The pH value was measured to analyze the hydrolytic stability of the sample after immersion in SBF. The initial pH of SBF was 7.4 for all samples.

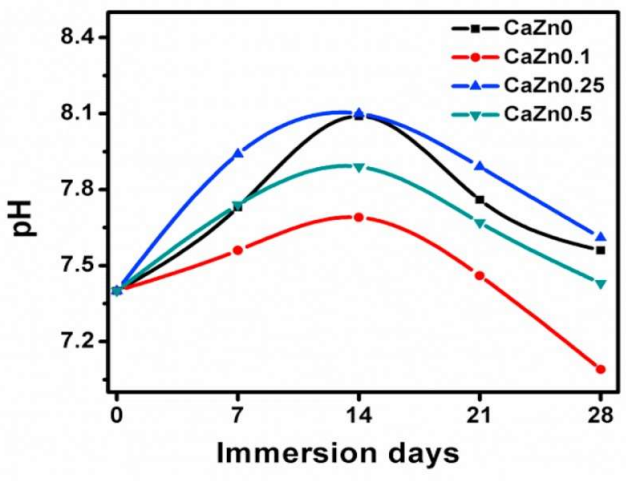

Figure 5.14 Variation in pH in SBF.

Initially, the pH increases for 14 days due to the exchange of Ca^{+}, Zr^{+}, and Zn^{+} of samples with ions of SBF (H^{+} or H_3O^{+}). Si^{+} ions presented in baghdadite form silanol group on the surface and induce negative charges on the surface. The Ca^{+2} and P^{+} ions are attracted to the surface and the apatite layer is formed on the surface (Najafinezhad et al, 2017, Schumacher et al., 2015). The formed apatite layer was confirmed by characterizing the sample using XRD and FTIR. The consumption of OH^{-} ions reduces the pH. The apatite layer was formed over the surface after 14 days of immersion in SBF. This behavior of pH was due to the ion exchange process.

Figure 5.15 shows the degradation of composite samples after immersion in SBF for a different period. It found that sample CaZn0 has an increasing degradation rate with immersing time and was about 4.59% after 28 days. The CaZn0 shows a small variation in

weight loss up to 21 days. After that, an increase in weight loss indicates that calcium zirconium silicate has a faster degradation rate than the other three samples. The increased degradation in calcium zirconium silicate has observed due to hydrophilic nature (Bakhsheshi-Rad et al., 2017). After 28 days of immersion, the calcium zirconium silicate has a higher degradation rate. Sample CaZn0.5 has the lowest degradation rate that concludes that the addition of zinc oxide reduces the degradation of calcium zirconium silicate. The sample CaZn0.5 firstly showed weight loss for 14 days and weight gain after that. The weight gain in SBF indicates the hydroxyapatite (HAp) deposition on the material surface (Xiong et al., 2013). The weight loss in samples after immersion in SBF takes due to the ionic exchange process between ions of sample and SBF. This process depends upon the sample composition and changes the pH of the surrounding media solution. Results indicate that degradation in static SBF was very slow. The obtained results show that zinc substitution can be used as additives to alter the degradation behavior of calcium zirconium silicate.

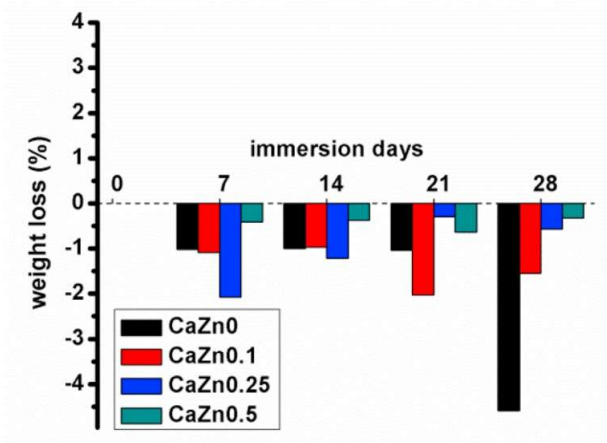

Figure 5.15 Weight loss in sample after immersion in SBF.

Figure 5.16 represents the water absorption of substituted calcium zirconium silicate with immersing time. The water absorption in zinc containing calcium zirconium silicate samples is higher than pure calcium zirconium silicate. The water absorption in samples CaZn0.25 and CaZn0.5 became almost constant after 7 days of immersion in SBF.

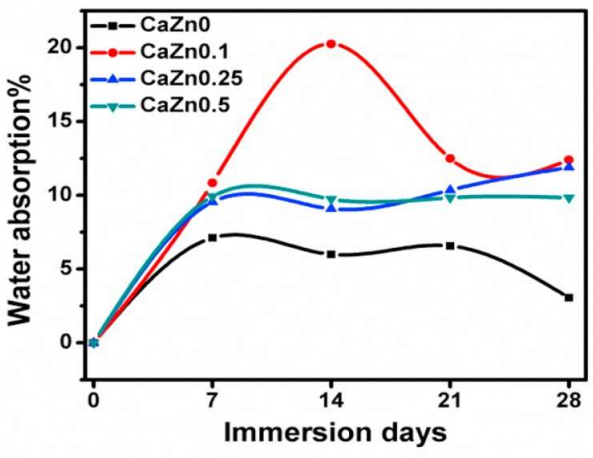

Figure 5.16 Water absorption in SBF.

5.15 Density

Figure 5.17 shows the bulk density of composite samples with sintering temperatures. With Zinc oxide, significant changes were observed in density and found improved with increasing zinc oxide amount. The bulk density increased in all samples until 800°C and decreased with increasing sintering temperature. The increment in density was observed because of compactness in powders with increasing temperature (Yadav et al., 2020).

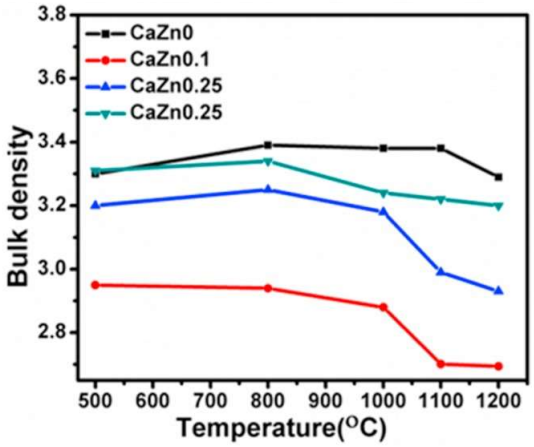

Figure 5.17 Bulk density with sintering temperature.

Figure 5.18 shows the compressive strength of samples sintered at 800°C. The result indicates that increasing the amount of zinc oxide in calcium zirconium silicate improves the compressive strength. From bulk density results, the density of pure calcium zirconium silicate is more than the other three and increased with zinc addition. The compressive strength depends upon the density and porosity; hence the compressive strength of pure calcium zirconium silicate is higher than the other three zinc-containing samples.

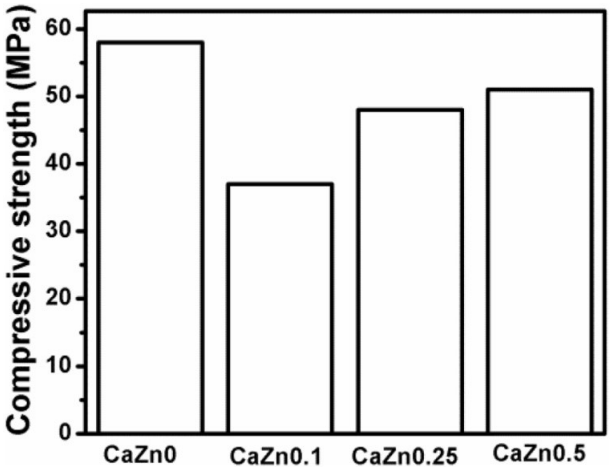

Figure 5.18 Compressive strength of samples after sintering at 800 °C. Data were presented in their average value.

5.16 In vitro blood compatibility

Hemocompatibility is a key parameter for any synthetic material for their biomedical applications. It measures the material's compatibility with blood (Ali et al., 2018). **Figure 5.19 (a)** shows the hemolysis rate (%) of the sample with varying zinc oxide amount at 50 mg/ml concentration. All samples show hemolysis rate <5% (1.88%, 2.01%, 3.16%, and 3.92% for sample CaZn0, CaZn0.1, CaZn0.25, and CaZn0.5 respectively) which confirmed their biocompatibility. No significant differences in the hemolysis rate found in CaZn0 and CaZn0.1 samples concerning each other. Whereas, the sample CaZn0.25 and CaZn0.5 showed a significant difference in hemolysis rate compared to CaZn0 and CaZn0.1. Further,

the sample CaZn0.5 with the highest concentration of zinc oxide showed the highest hemolysis rate than the other three samples within the limit. **Figure 5.19 (b)** shows the images of the micro-centrifuge tube when incubated with composites. It observed that ACD blood cells were hemolysed on exposure to the distilled water (positive control). With increasing zinc oxide in composite, the number of hemolysed blood cells was significantly lower compared to the positive control **(Figure 5.19 (c))**.

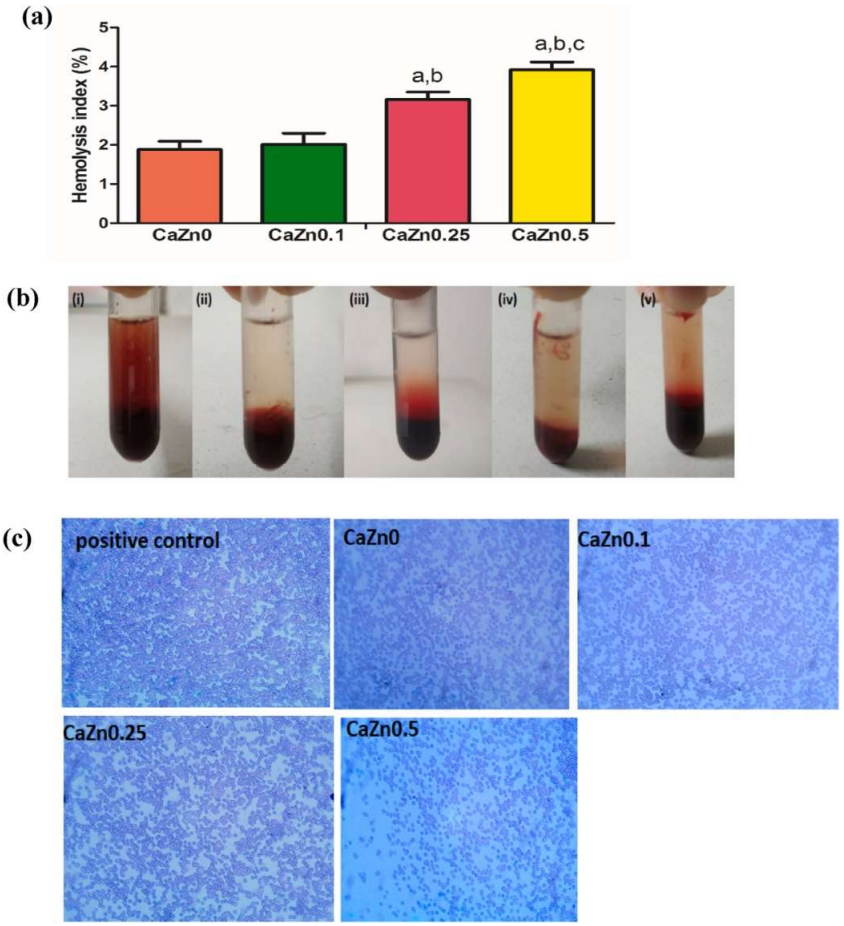

Figure 5.19 Hemocompatibility of baghdadite and zinc oxide doped baghdadite **(a)** histograms, The "a", "b", and "c" letters show the significant difference with respect to CaZn0, CaZn0.1 and CaZn0.25. **(b)** Microcentrifuge tubes **(i)** positive control, **(ii)** CaZn0, **(iii)** CaZn0.1, **(iv)** CaZn0.25, and **(v)** CaZn0.5, and **(c)** micrograph images of samples treated with ACD blood.

5.17 Apoptosis analysis

Figure 5.20 shows the DAPI behaviour of composites on MG63 cell lines after 24 h of the incubation period. After treating with a fixed concentration of composites, DAPI stains the nucleus of the viable cells after 24 h of incubation over the MG63 cell lines. The cell nucleus of composites is showed by the blue fluorescence of DAPI. The result shows a large number of spherical cells attached to the surface of baghdadite which show its affinity towards MG63 cells. Due to the short incubation period (24 h), cells have insufficient time to infiltrate inside the surface and seeded only on the external surface of the samples. However, in zinc oxide containing baghdadite composites, the number of cells attached on the surface reduces with an increasing the amount of zinc oxide amount.

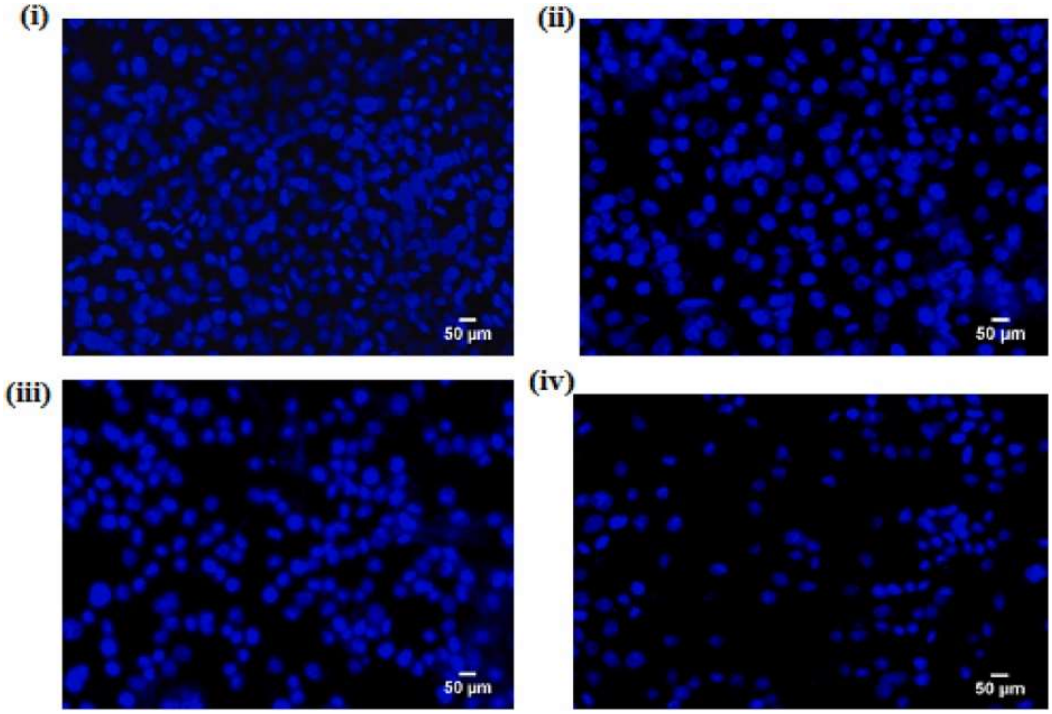

Figure 5.20 Apoptosis of cells following treatment with fixed concentration of (i) CaZn0, (ii) CaZn0.1, (iii) CaZn0.25, and (iv) CaZn0.5. The treated cells were stained with DAPI. Blue color staining with DAPI suggests the living and healthy cells. (For interpretation of the references to color in this figure legend, the reader is referred to the Web version of this article.)

5.18 Antibacterial test

The antibacterial viability of composites over *E. Coli* and *S. Aureus* bacterial strain shown in **Figure 5.21** Results indicate that the viability of *E. coli* and *S. Aureus* bacteria decreases with zinc oxide addition in calcium zirconium silicate. The bacterial viability of *S. aureus* bacteria reduces with increasing zinc oxide amount by 2.95 %, 21.17 %, 26.78 %, and for *E. coli* bacteria, it shows a drop by 9.92 %, 23.47 %, 37.16 % as compared to pure calcium zirconium silicate. The antibacterial mechanism for zinc oxide is still unclear. Some researchers reported that the generation of hydrogen peroxide and leaching of zinc ion into media are responsible for antibacterial behavior in zinc oxide (Aydin et al., 2010). These findings suggest that the antibacterial response of the material depends upon the dopant amount and type of bacteria. The antibacterial effect of *E. coli* and *S. Aureus* bacterial strain on composites were also calculated and found increasing with zinc oxide addition as compared to pure calcium zirconium silicate and found 12.39 %, 15 %, 30.94 %, and 35.86 % against *S. Aureus* and 14.33 %, 22.83 %, 34.44 %, 46.17 % against *E. coli* for CaZn0, CaZn0.1, CaZn0.25, and CaZn0.5 samples.

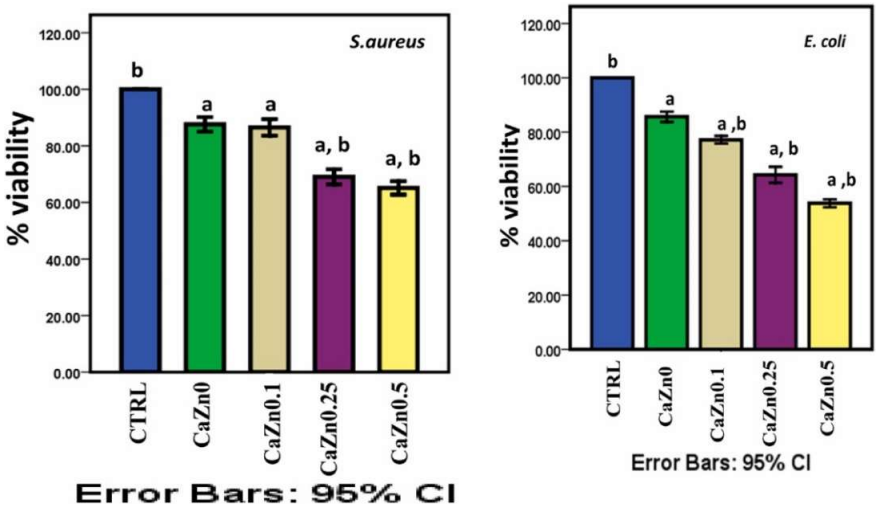

Figure 5.21 Shows the viability of S.aureus and E.coli on samples. Data were presented in mean ± SD (n = 3). Letters "a" and "b" present the statistical difference (p value < 0.05) among all samples with respect to control and CaZn0 respectively.

5.19 Conclusions

In this study, the aim was to improve the biological properties of baghdadite ceramic using the substitution of zinc ion into baghdadite crystal structure. For this, zinc oxide substituted baghdadite was synthesized by a solid-state ceramic synthesis route. For the synthesis, raw materials were taken in their corresponding molar ratio without considering their weight loss. A reduction in synthesis temperature was found due to incorporation of ZnO. Optimum sintering temperature was selected to achieve maximum relative density. With increasing zinc oxide content, compressive strength and density of composites have improved. All composites show the formation of the crystalline apatite layer with a controlled degradation rate in SBF. The antibacterial results suggest that the antibacterial performance of baghdadite/zinc oxide composite was dependent upon the zinc oxide content in the composite. Composite with higher zinc oxide amount shows a higher antibacterial effect and

more effective against *E. Coli*. The hemolysis rate was found <5 % for blood compatibility of the composite. The DAPI staining on MG63 cells shows the good attachment of cells over the baghdadite surface. The obtained results suggest that zinc oxide-containing baghdadite composite is a potential material for biomedical application.